

Supplemental Information

MicroRNA governs bistable cell differentiation and lineage segregation via a noncanonical feedback

Chung-Jung Li^{1,2}, Ee Shan Liao^{1,2}, Ziyi Liu³, Andrew Willems³, Victoria Garside⁴, Edwina McGlinn⁴, Jun-An Chen^{1,2}, Tian Hong^{5,6},

1. Molecular and Cell Biology, Taiwan International Graduate Program, Academia Sinica and Graduate Institute of Life Science, National Defense Medical Center, Taipei, Taiwan.

2. Institute of Molecular Biology, Academia Sinica, Taipei, 11529, Taiwan.

3. Genome Science and Technology Program, The University of Tennessee, Knoxville, Tennessee, USA.

4. EMBL Australia, Australian Regenerative Medicine Institute, Monash University, Clayton, Victoria, Australia.

5. Department of Biochemistry & Cellular and Molecular Biology, The University of Tennessee, Knoxville, Tennessee, USA.

6. National Institute for Mathematical and Biological Synthesis, Knoxville, Tennessee, USA.

Table of Contents

1. Mathematical models and analysis	3
1.1 List of all models	3
1.2 Transcriptional cross repression (T-CR) Model	3
1.3 Transcriptional unilateral repression (T-UR) Model	5
1.4 Transcriptional unilateral repression with miRNA regulation (Tmi-UR) Model	5
1.5 Transcriptional unilateral repression with transcription and miRNA mediated feedback (Tmi-FB) Model	7
1.6 Performance evaluation of spatiotemporal models.	7
1.7 mRNA-miRNA model with one binding site (mmi-1 Model).....	9
1.8 mRNA-miRNA model with two binding sites (mmi-2 Model)	10
1.8.1 Model construction and simplification.....	10

34	1.8.2 Analysis of the number of steady states.....	13
35	1.8.3 Numerical experiments for bistable switches	15
36	1.9 mRNA-miRNA model with three binding sites (mmi-3 Model).....	17
37	1.10 Estimate of realistic biological circuits described by mmi-2 and mmi-3 Models.....	18
38	1.11 mRNA-miRNA with noncanonical feedback and morphogen gradients (mmi-S Model).....	18
39	1.12 List of parameter values and ranges for random sampling	18
40	2. Additional Information of Resources.....	20
41	2.1 List of key reagents and resources	20
42	2.2 Primers for genotyping	22
43	2.3 Sequence for miRNA sponge.....	23
44	Supplemental References.....	24
45		
46		
47		

1. Mathematical models and analysis

1.1 List of all models

Table S1 summarizes the information of all mathematical models in this study. The subsequent sections describe these models in detail.

Table S1. List of all models

Model abbreviation	Model full name	Morphogen gradient	Presenting figure	Text with details
T-CR	Transcriptional cross repression	Included	Figure 2	Supplementary Text 1.2
T-UR	Transcriptional unilateral repression	Included	Figure S2	Supplementary Text 1.3
Tmi-UR	Transcriptional unilateral repression with miRNA regulation	Included	Figure 4	Supplementary Text 1.4
Tmi-FB	Transcriptional unilateral repression with transcription and miRNA mediated feedback	Included	Figure 4	Supplementary Text 1.5
mmi-1	mRNA-miRNA with one binding site	Not included	Figure 5	Supplementary Text 1.7
mmi-2	mRNA-miRNA with two binding sites	Not included	Figure 5	Supplementary Text 1.8
mmi-3	mRNA-miRNA with three binding sites	Not included	Figure 5	Supplementary Text 1.9
mmi-S	mRNA-miRNA with noncanonical feedback and morphogen gradients	Included	Figure 8	Supplementary Text 1.11

1.2 Transcriptional cross repression (T-CR) Model

To understand the segregation of $Hoxa5^{on}Hoxc8^{off}$ and $Hoxa5^{off}Hoxc8^{on}$ motor neurons (MNs), we first considered a canonical model of transcriptional cross repression (T-CR) between $Hoxa5$ and $Hoxc8$. The model consists of 40 compartments (cells) describing discretized space spanning the rostral-caudal axis of the developing spinal cord. In each compartment, the lineage decision of each cells is governed by the following ordinary differential equations (ODEs):

$$\frac{dR_5}{dt} = s_5^0 + s_5 \frac{(A(t)/K_{5A})^{n_{5A}}}{1 + (A/K_{5A})^{n_{5A}} + (P_8/K_{58})^{n_{58}}} - k_5 R_5 \quad (1a)$$

$$\frac{dR_8}{dt} = s_8^0 + s_8 \frac{(F(t)/K_{8F})^{n_{8F}}}{1 + (F/K_{8F})^{n_{8F}} + (P_5/K_{85})^{n_{85}}} - k_8 R_8 \quad (1b)$$

$$\frac{dP_5}{dt} = l_5^0 R_5 - P_5 \quad (1c)$$

$$\frac{dP_8}{dt} = l_8^0 R_8 - P_8 \quad (1d)$$

66

67 Here, R_5 , P_5 , R_8 , P_8 represent the concentration of *Hoxa5* mRNA, Hoxa5 protein, *Hoxc8* mRNA and
 68 Hoxc8 protein, respectively. s_5^0 and s_8^0 are the transcription factors independent (basal) production rate
 69 constants of *Hoxa5* mRNA and *Hoxc8* mRNA, respectively. K_{XY} represents the apparent threshold of
 70 activation or inhibition of mRNA X by transcription factor Y , and n_{XY} describes the nonlinearity of the
 71 same transcriptional regulation. k_5 and k_8 are the degradation rate constants of *Hoxa5* mRNA and *Hoxc8*
 72 mRNA, respectively. l_5^0 and l_8^0 are the translation rate constants of free forms of *Hoxa5* mRNA and *Hoxc8*
 73 mRNA, respectively. Although it is unnecessary to model protein and mRNA dynamics separately for the
 74 demonstration of lineage decision and boundary formation in this case, we considered mRNA and protein
 75 dynamics explicitly to keep the model consistent with other models in this study.

76 A and F are the concentrations of RA and FGF respectively, and their dynamics are governed by the simple
 77 reaction-diffusion system $\partial_t X = D \partial_x^2 X - kX$, where X is the concentration of RA or FGF (A or F), D is
 78 the diffusion coefficient, and k is the degradation rate constant. We assumed that the RA and FGF are
 79 synthesized at the rostral boundary and caudal boundary respectively, and the non-synthesizing boundaries
 80 have no flux. We assumed that D and k are relatively fast with respect to intracellular kinetics so the system
 81 is approximated by steady solution of the reaction-diffusion system which has an antiparallel, exponential
 82 decay pattern of RA and FGF along the RC axis. We approximated the RC axis of the tissue by 40
 83 compartments, and dynamics of A or F in the i th compartment along the axis are approximated by:

84

$$\frac{dA_i}{dt} = \gamma_A (m_A e^{\sigma_A i} - A_i) \quad (2a)$$

$$\frac{dF_i}{dt} = \gamma_F (m_F e^{\sigma_F (L-i)} - F_i) \quad (2b)$$

87

88 γ_A and γ_F represent the timescales of the RA and FGF dynamics (assumed to be 1). σ_A and σ_F are length
 89 scale constants (assumed to be 0.01) determined by D and k of the morphogens. L is the width of the
 90 modeled space (40 units). m_A and m_F are the levels of RA at the rostral boundary and FGF at the caudal
 91 boundary of the modeled space, respectively. These two parameters were assumed to be time dependent to
 92 reflect realistic RA and FGF dynamics that are most plausible during development: m_A and m_F were
 93 assumed to increase abruptly during the early spinal cord development (the increase of m_A from 0 to 2.1
 94 was followed by the increase of m_F from 0 to 2.3), and then gradually declined (m_A and m_F were reduced
 95 to 65% of their maximal values, and γ_A and γ_F were decreased from 1 to 0.005). The assumed dynamics
 96 can be explained by the rapid activation of RA synthesis at the rostral end of the embryo, followed by FGF
 97 synthesis activation at the caudal end, and the subsequent expansion of the embryo along the rostral-caudal
 98 axis. Although the dynamics of RA and FGF are difficult to measure in the mouse spinal cord, transient
 99 morphogen signals are consistent with previous observations (Ensini *et al*, 1998; Mazzoni *et al*, 2013). In

addition, we considered temporal fluctuations of RA and FGF signaling by introducing a moderate amount of noise when we simulated Eq 2. The positional information encoded by steady state RA concentration was previously reported to be noisy and shallow in zebrafish (Sosnik *et al*, 2016). Each derivative in Eq 2 has an additional noisy input εX , where X is the concentration of RA or FGF (A or F), and $\varepsilon = 0.001 \cdot N(0,1)$. $N(0,1)$ is a random number drawn from a normal distribution with mean of 0 and unit variance. During the simulations, a random number was drawn every 5 time units after time 300.

1.3 Transcriptional unilateral repression (T-UR) Model

Experimental evidence has suggested that *Hoxc8* inhibits *Hoxa5* in a unilateral fashion (Dasen *et al*, 2005; Philippidou & Dasen, 2013) (this study). Therefore, the T-CR Model is unlikely valid. To model the MN differentiation with a more realistic gene regulatory network (GRN), we modified Eq 1 by simplify removing the repression of *Hoxc8* transcription by *Hoxa8*, and considered the following ODEs to describe the *Hoxa5* and *Hoxc8* dynamics:

$$\frac{dR_5}{dt} = s_5^0 + s_5 \frac{(A(t)/K_{5A})^{n_{5A}}}{1 + (A/K_{5A})^{n_{5A}} + (P_8/K_{58})^{n_{58}}} - k_5 R_5 \quad (3a)$$

$$\frac{dR_8}{dt} = s_8^0 + s_8 \frac{(F(t)/K_{8F})^{n_{8F}}}{1 + (F/K_{8F})^{n_{8F}}} - k_8 R_8 \quad (3b)$$

$$\frac{dP_5}{dt} = l_5^0 R_5 - P_5 \quad (3c)$$

$$\frac{dP_8}{dt} = l_8^0 R_8 - P_8 \quad (3d)$$

The descriptions of variables and parameters are identical to the T-CR Model. Several adjustments of parameter values were made to achieve clear segregation of *Hoxa5*^{on} and *Hoxc8*^{on} MNs in the presence of noise-free morphogen signals.

1.4 Transcriptional unilateral repression with miRNA regulation (Tmi-UR) Model

To consider post-transcriptional regulation, we incorporated two miRNAs, miR-27 and miR-196, into the T-UR model. miR-27 and miR-196 control the expression of *Hoxa5* and *Hoxc8* respectively (Li *et al*, 2017; Wong *et al*, 2015). The modeling framework is based on previous studies concerning miRNA regulations (Lu *et al*, 2013; Osella *et al*, 2011). In this framework, miRNAs inhibit protein production via inducing mRNA degradation and translational repression upon binding to the 3' UTR of the target mRNAs. The 3' UTR of *Hoxa5* mRNA has three conserved putative binding sites for miR-27, whereas that of the *Hoxc8* mRNA has four conserved putative binding sites for miR-196 (this study). The intracellular system is described by the following ODEs:

$$\frac{dR_5}{dt} = s_5^0 + s_5 \frac{(A(t)/K_{5A})^{n_{5A}}}{1 + (A/K_{5A})^{n_{5A}} + (P_8/K_{58})^{n_{58}}} - k_5(R_5 - \sum_{i=1}^3 \binom{3}{i} C_5^i) - \sum_{i=1}^3 k_5^i \binom{3}{i} C_5^i \quad (4a)$$

$$\frac{dR_8}{dt} = s_8^0 + s_8 \frac{(F(t)/K_{8F})^{n_{8F}}}{1 + (F/K_{8F})^{n_{8F}}} - k_8(R_8 - \sum_{i=1}^4 \binom{4}{i} C_8^i) - \sum_{i=1}^4 k_8^i \binom{4}{i} C_8^i \quad (4b)$$

$$\frac{dP_5}{dt} = l_5^0(R_5 - \sum_{i=1}^3 \binom{3}{i} C_5^i) + \sum_{i=1}^3 l_5^i \binom{3}{i} C_5^i - P_5 \quad (4c)$$

$$\frac{dP_8}{dt} = l_8^0(R_8 - \sum_{i=1}^4 \binom{4}{i} C_8^i) + \sum_{i=1}^4 l_8^i \binom{4}{i} C_8^i - P_8 \quad (4d)$$

$$\frac{dr_2}{dt} = s_2 \frac{1}{1 + (A/K_{2A})^{n_{2A}}} - k_2(r_2 - \sum_{i=1}^3 i \binom{3}{i} C_5^i) - \sum_{i=1}^3 i k_2^i \binom{3}{i} C_5^i \quad (4e)$$

$$\frac{dr_9}{dt} = s_9 - k_9(r_9 - \sum_{i=1}^4 i \binom{4}{i} C_8^i) - \sum_{i=1}^4 i k_9^i \binom{4}{i} C_8^i \quad (4f)$$

139

140 Here, R_5 and R_8 are the total concentrations of *Hoxa5* and *Hoxc8* mRNAs, respectively, including those
 141 bound by miRNAs and free mRNAs. r_2 and r_9 are the total concentrations of miR-27 and miR-196,
 142 respectively. l_5^i and k_5^i are the translation rate constant and degradation rate constant of *Hoxa5* mRNA
 143 when i numbers of miR-27 bind to it, respectively. k_2^i is the degradation rate constant of miR-27 in these
 144 complexes. l_8^i and k_8^i are the translation rate constant and degradation rate constant of *Hoxc8* mRNA when
 145 i numbers of miR-196 bind to it, respectively. k_9^i is the degradation rate constant of miR-196 in these
 146 complexes. s_2 and s_9 are the maximal production rate constants of miR-27 and miR-196 respectively. k_2
 147 and k_9 are the degradation rate constants of free forms of miR-27 and miR-196 respectively.

148 $\sum_{i=1}^3 i \binom{3}{i} C_5^i = 3C_5^1 + 2 \cdot 3C_5^2 + 3C_5^3$, and this represents the total amount of miR-27 bound to *Hoxa5*
 149 mRNA. Each term of this summation describes $\binom{3}{i}$ scenarios in which i number of miRNA molecules bind
 150 to 3 possible binding sites that each *Hoxa5* mRNA has. $\sum_{i=1}^3 \binom{3}{i} R_{5i} = 3C_5^1 + 3C_5^2 + C_5^3$, and this represents
 151 the total amount of complex formed by miR-27 and *Hoxa5* mRNA. The complexes for miR-196 bound
 152 *Hoxc8* mRNA are defined similarly: $\sum_{i=1}^4 \binom{4}{i} C_8^i = 4C_8^1 + 6C_8^2 + 4C_8^3 + C_8^4$, and so are the total amount of
 153 miR-196 bound to *Hoxc8* mRNA: $\sum_{i=1}^4 i \binom{4}{i} C_8^i = 4C_8^1 + 2 \cdot 6C_8^2 + 3 \cdot 4C_8^3 + 4C_8^4$. The concentrations of
 154 these complexes are determined by the following algebraic equations:

$$C_5^1 = \kappa_5^1(r_2 - \sum_{i=1}^3 i \binom{3}{i} C_5^i) (R_5 - \sum_{i=1}^3 \binom{3}{i} C_5^i) \quad (5a)$$

$$C_5^i = \kappa_5^i(r_2 - \sum_{j=1}^3 j \binom{3}{j} C_5^j) C_5^{i-1} \quad i = 2, 3 \quad (5b)$$

$$C_8^1 = \kappa_8^1 (r_9 - \sum_{i=1}^4 i \binom{4}{i} C_8^i) (R_8 - \sum_{i=1}^4 \binom{4}{i} C_8^i) \quad (5d)$$

$$C_8^i = \kappa_8^i (r_9 - \sum_{j=1}^4 j \binom{4}{j} C_8^j) C_8^{i-1} \quad i = 2, 3, 4 \quad (5e)$$

κ_5^i and κ_8^i are the inverse of the dissociation constants (i.e. association constants) for complex formation of C_5^i and C_8^i respectively.

This modeling framework has been used to model miRNA mediated feedforward loops, as well as feedback loops involving transcriptional inhibition of miRNAs by transcription factors (Lu *et al.*, 2013; Osella *et al.*, 2011). In this study, we took advantage of this successful framework for building all of our models involving miRNAs. However, we addressed a key limitation of the previous modeling framework: the degradation rate constants of each mRNA or miRNA in multiple complexes (i.e. k_X^i where X is any mRNA or miRNA, and $i \geq 1$) were assumed to be identical (Lu *et al.*, 2013; Osella *et al.*, 2011). This assumption is inconsistent with several experimental studies (de la Mata *et al.*, 2015; Ghini *et al.*, 2018; Grimson *et al.*, 2007). A previous modeling study by Tian *et al.* relaxed this assumption in certain parameter region, and reported a possible bistable arising from purely post-transcriptional reactions (Tian *et al.*, 2016). However, systematic analysis of k_X^i and comparison with experimental data were not performed. In this study, we relaxed this assumption with systematic analysis of the effect of differential k_X^i in multiple mRNA-miRNA complexes (1.7-1.9).

1.5 Transcriptional unilateral repression with transcription and miRNA mediated feedback (Tmi-FB) Model

The Tmi-FB model extends the Tmi-UR model by assuming transcriptional repression of miR-27 by Hoxa5, and repression of miR-196 by Hoxc8, i.e. replace Eq 4e and 4f by the following ODEs:

$$\frac{dr_2}{dt} = s_2 \frac{1}{1 + (A/K_{2A})^{n_{2A}} + (P_5/K_{25})^{n_{25}}} - k_2 (r_2 - \sum_{i=1}^3 i \binom{3}{i} C_5^i) - \sum_{i=1}^3 i k_5^i \binom{3}{i} C_5^i \quad (5a)$$

$$\frac{dr_9}{dt} = s_9 \frac{1}{1 + (P_8/K_{98})^{n_{98}}} - k_9 (r_9 - \sum_{i=1}^4 i \binom{4}{i} C_8^i) - \sum_{i=1}^4 i k_8^i \binom{4}{i} C_8^i \quad (5b)$$

All other equations are identical to Eq 2, Eq 4 and Eq 5. A hypothetical inhibition of miR-27 by Hoxa5 is described by K_{25} (threshold) and n_{25} (cooperativity). Similarly, a hypothetical inhibition of miR-196 by Hoxc8 is described by K_{98} (threshold) and n_{98} (cooperativity). Neither of these transcriptional inhibitions is supported by experimental data.

1.6 Performance evaluation of spatiotemporal models.

To evaluate T-CR, T-UR, Tmi-UR and Tmi-FB Models in terms of their capacity of governing cell lineage segregation at the tissue boundary and their consistency with experimental observations, we performed numerical simulations and analysis of the four models with the following scheme:

1. Simulation procedure: We used a 10X40 grid representing 400 cells for each model. These cells receive various levels of RA and FGF signals based on their indices of columns which represent the positions along the RC axis. In each simulation, RA and FGF signals in all cells were rapidly increased at time 50 and 100 respectively to its maximum levels (see 1.2), and then starting from time 150 (RA) and time 200 (FGF) slowly decreased to 65% of their maximum levels. This dynamic profile reflects the possible morphogen dynamics during development, which has not been measured experimentally. The RA and FGF signals were also subject to moderate temporal fluctuations in all cells (see 1.2). At time 1000, all state variables have approached their steady states. Time evolutions of the lineage defining molecules Hoxa5 and Hoxc8 proteins obtained from four representative simulations are shown in Movies S1-S4.

2. Parameter sampling: To ensure that the performance evaluations were not sensitive to the choice of parameters, we chose 10000 parameter sets randomly for each model, except for a few parameters which were assumed to be the same constants across all models. For gene regulations common to multiple models, the corresponding parameter values were chosen from the same log-normal distributions with μ and σ values listed in Table S3. Because we were interested in the upper bound of performance of each model, all nonlinearity parameter (n) was set to 6, which is biological plausible under physiological conditions. For each model, one representative parameter set was chosen and adjusted manually to show simulation trajectories and patterns of cellular distributions. Other analyses were performed based on the results from all sampled parameter sets.

3. Performance of lineage segregation: We analyzed the distributions of all simulated molecules at time 1000. To quantify the lineage decision performance at the tissue boundary, we used the Transition Width (W) defined as the number of columns in the 10X40 grid where one or more elements (cells) have undetermined lineage at the final time point (1000). To define the lineage decision, we first define molecule X is expressed in a cell when its level at time 1000 is higher than 5% of the maximum level of X across all cells in the domain at the same time point. If a column of cells in the domain satisfies at least one of the following conditions, the column is counted toward W : 1) at least one cell expresses both Hoxa5 and Hoxc8; 2) at least one cell expresses neither Hoxa5 nor Hoxc8; 3) the column has both Hoxa5^{on}Hoxc8^{off} and Hoxa5^{off}Hoxc8^{on} cells. Because this procedure does not guarantee a meaningful boundary, we further constrain W by enforcing that at least one adjacent column pair has a difference in either Hoxa5 and Hoxc8 higher than 35% of the overall change across the domain (i.e. between rostral end and caudal end). If this condition is not satisfied, W is set to the maximum (40). A model has a desirable performance when $W = 0$. Out of the four models, T-CR and Tmi-FB Models had some of the sampled parameter sets that produced transition width of zero (4.4% and 1.97% respectively out of 10000), whereas the other two models did not have any parameter set that achieved this performance.

3. Difference between segregations of mRNAs and proteins. Because we observed a clear cell-to-cell segregation of Hoxa5 and Hoxc8 proteins at the boundary, but not their mRNAs, a key metric to evaluate the models is the differential segregation degrees of mRNAs and proteins. To describe this performance, we used a segregation index $S = \frac{\sup(\Delta R_S) + \sup(\Delta P_S)}{\sup(\Delta P_S) + \sup(\Delta P_S)}$, where ΔX is a vector representing the ratios of mean levels of X between all 39 adjacent column pairs in the domain. We define that a model has a desirable performance when $S < 0.2$. Out of the four models, Tmi-UR and Tmi-FB Models had some of the sampled parameter sets that produced $S < 0.2$ (0.018% and 11.26% respectively out of 10000 sets), whereas the other two models did not have any parameter set that achieved this performance.

Using the criterion based on W and S , 190 parameter sets were selected, and all of them were from the Tmi-FB Model. By analyzing the miR-196 distributions from the simulations with these parameter sets, we found that all of the simulations had very low levels (<0.01) of miR-196 at the caudal boundary of this domain, an observation inconsistent with published experimental data (Kloosterman *et al*, 2006; Wong *et al.*, 2015).

1.7 mRNA-miRNA model with one binding site (mmi-1 Model)

To analyze mRNA-miRNA interactions at a more fundamental level, we revisit the biochemical reactions underpinning models describing the interactions, e.g. the Tmi-UR Model. We first considered a model describing concentrations of a miRNA and an mRNA (target) with one binding site for the miRNA. The full reaction network is as follows:



Here, R is the concentration of the free mRNA. r is the concentration of the free miRNA. C is the concentration of the partially double-stranded RNA molecule formed by partial complementarity of one miRNA molecule and one mRNA molecule. For simplicity, this type of RNA molecule is also called complex in this study. s_R is the synthesis rate constant of mRNA. k_R^0 is the degradation rate constant of free mRNA. s_r is the synthesis rate constant of miRNA. k_r^0 is the degradation rate constant of free miRNA. k_R^1 is the degradation rate constant of mRNA in the complex. k_r^1 is the degradation rate constant of miRNA in the complex. K is the dissociation constant of the binding of miRNA to mRNA. It is the ratio between the rate constant for complex dissociation (k_C^{off}) and that for miRNA-mRNA binding (k_C^{on}).

We applied Chemical Reaction Network Theory (CRNT) with these reactions and found that the system cannot be bistable (Feinberg, 2019). To confirm this result and to provide a foundation for more complex models, we used the following ODEs to describe the reactions with the law of mass action:

$$\frac{dR}{dt} = s_R - k_R^0 R - k_C^{\text{on}} R r + k_C^{\text{off}} C + k_r^1 C \quad (6a)$$

$$\frac{dr}{dt} = s_r - k_r^0 r - k_C^{\text{on}} R r + k_C^{\text{off}} C + k_R^1 C \quad (6b)$$

$$\frac{dC}{dt} = k_C^{\text{on}} R r - k_C^{\text{off}} C - k_r^1 C - k_R^1 C \quad (6c)$$

We next used total quasi-steady state approximation (tQSSA) to reduce the number of ODEs (Borghans *et al*, 1996; Ciliberto *et al*, 2007). This approximation assumes that the binding and unbinding rate constants $k_C^{\text{off}}, k_C^{\text{on}}$ are much greater than other rate constants. As such, the reaction $R + r \leftrightarrow C$ is always at steady state any at given t . The new ODEs describe slow reactions concerning the total concentrations of mRNA and miRNA only:

$$\frac{dR_T}{dt} = s_R - k_R^0 R - k_R^1 C \quad (7a)$$

$$\frac{dr_T}{dt} = s_r - k_r^0 r - k_r^1 C \quad (7b)$$

The concentrations of individual molecules r , R and C are determined by the following equation:

$$\begin{aligned} k_C^{\text{off}} C &= k_C^{\text{on}} Rr \\ \Leftrightarrow KC &= Rr \end{aligned} \quad (8)$$

Eq 8 indicates that $\{R, r, C\}$ are at steady state at any given t . This implies that these three variables are bounded for any bounded $\{R_T, r_T\}$ at any given t . We next show that this system described by Eq 7 and Eq 8 cannot be bistable. A bistable system is defined as a system with two stable steady states and one unstable steady state. The steady state of system is governed by:

$$0 = s_R - k_R^0 R - k_R^1 C \quad (9a)$$

$$0 = s_r - k_r^0 r - k_r^1 C \quad (9b)$$

$$0 = KC - Rr \quad (9c)$$

Solving Eq 9a and b for R and r respectively, and substituting them in Eq 9c yields:

$$\frac{k_r^1 k_R^1 C^2 - (K k_R^0 k_r^0 + k_r^1 s_R + k_R^1 s_r) C + s_R s_r}{k_R^0 k_r^0} = 0 \quad (10)$$

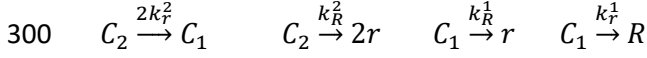
Since the numerator is a quadratic polynomial and the denominator is a positive constant, the equation has at most two real solutions. Therefore, the system described by Eq 7 and Eq 8 cannot be bistable. We concluded that the elementary interactions involving a miRNA and an mRNA with only one miRNA binding site do not allow bistable switches.

1.8 mRNA-miRNA model with two binding sites (mmi-2 Model)

1.8.1 Model construction and simplification

We next considered a model describing concentrations of a miRNA and an mRNA (target) with two binding sites for the miRNA. The full reaction network is as follows:





301

302 Here, C_1 is the concentration of the partially double-stranded RNA molecule formed by partial
 303 complementarity of one miRNA and one mRNA molecules (1:1 complex). Note that this complex has two
 304 forms because of the two binding sites. For simplicity, we assumed that the two binding sites are equivalent
 305 throughout this study. C_2 is the concentration of the partially double-stranded RNA molecule formed by
 306 partial complementarity of one miRNA and one mRNA molecules (2:1 complex). K_1 and K_2 are the
 307 dissociation constants for the two complexes respectively. k_R^1 is the degradation rate constant of mRNA in
 308 the 1:1 complex. k_r^1 is the degradation rate constant of miRNA in the 1:1 complex. k_R^2 is the degradation
 309 rate constant of mRNA in the 2:1 complex. k_r^2 is the degradation rate constant of miRNA in the 2:1 complex.
 310 Other notations are described in 1.7. Similar to the mmi-1 Model, a key underlying assumption is that
 311 miRNA and mRNA are degraded independently from their partially double-stranded forms.

312 We describe the reactions with the law of mass action and the tQSSA using the following differential
 313 algebraic equations:

314

$$315 \quad \frac{dR_T}{dt} = s_R - k_R^0 R - 2k_R^1 C_1 - k_R^2 C_2 \quad (11a)$$

$$316 \quad \frac{dr_T}{dt} = s_r - k_r^0 r - 2k_r^1 C_1 - 2k_r^2 C_2 \quad (11b)$$

$$317 \quad 0 = Rr - K_1 C_1 \quad (11c)$$

$$318 \quad 0 = C_1 r - K_2 C_2 \quad (11d)$$

$$319 \quad 0 = R + 2C_1 + C_2 - R_T \quad (11e)$$

$$320 \quad 0 = r + 2C_1 + 2C_2 - r_T \quad (11f)$$

321

322 Here, Eq 11a and b describe slow processes (synthesis and degradation) that control the changes of the state
 323 variables, whereas Eq 11c-f govern the concentrations of molecules that are determined by fast processes,
 324 i.e. binding and unbinding. Eq 11c-f indicate that $\{R, r, C_1, C_2\}$ are at steady state at any given t . This
 325 implies that these four variables are bounded for any bounded $\{R_T, r_T\}$ at any given t . To reduce the number
 326 of parameters, we considered a scaled independent variable $\tau = k_R^0 t$. We assumed that $k_R^0, s_R > 0$ (non-
 327 zero production rate and degradation rate constants of R), and we defined $\gamma = k_r^0/k_R^0$, $\mu = s_r/s_R$,
 328 $k_R^1 = a_1 k_R^0$, $k_R^2 = a_2 k_R^0$, $\bar{s}_R = s_R/k_R^0$, $\bar{R}_T = R_T/\bar{s}_R$, $\bar{r}_T = r_T/\bar{s}_R$, $\bar{C}_1 = C_1/\bar{s}_R$, $\bar{C}_2 = C_2/\bar{s}_R$. The ODEs in
 329 Eq 11 can be rewritten as follows:

330

$$331 \quad k_R^0 \bar{s}_R \frac{d\bar{R}_T}{d\tau} = k_R^0 \bar{s}_R - k_R^0 \bar{s}_R (\bar{R} + 2a_1 \bar{C}_1 + a_2 \bar{C}_2)$$

$$332 \quad k_R^0 \bar{s}_R \frac{d\bar{r}_T}{d\tau} = s_r - k_r^0 \bar{s}_R (\bar{r} + 2b_1 \bar{C}_1 + 2b_2 \bar{C}_2)$$

333

$$\Leftrightarrow \frac{d\bar{R}_T}{d\tau} = 1 - (\bar{R} + 2a_1\bar{C}_1 + a_2\bar{C}_2) \quad (12a)$$

$$\frac{d\bar{r}_T}{d\tau} = \mu - \gamma(\bar{r} + 2b_1\bar{C}_1 + 2b_2\bar{C}_2) \quad (12b)$$

Here, a_1 and a_2 are the fold-changes of degradation rate constant of mRNA upon miRNA binding with respect to free mRNA. b_1 and b_2 are the fold-changes of degradation rate constant of miRNA upon mRNA binding with respect to free miRNA.

We assumed that the miRNA regulates the mRNA when the mRNA is actively synthesized (an ‘on-state’ of the gene). Suppose at a steady state where no miRNA is produced ($s_r = r_T = C_1 = C_2 = 0$), and R_T represents a molar concentration in the range of $(10^{-9}, 10^{-7})$ M at this steady state (Lahtvee *et al*, 2017), then the approximate range of \bar{s}_R is given by: $\bar{s}_R = s_R/k_R^0 = k_R^0 R_T/k_R^0 = R_T \in (10^{-9}, 10^{-7})$ M. The estimated value of \bar{R}_T at this state (without miRNA regulation) is given by $\bar{R}_T = R_T/\bar{s}_R = R_T/R_T = 1$.

For simplicity, we dropped the bars in Eq 11 and we rewrote the system defined in Eq 11 as follows:

$$\dot{R}_T = 1 - (R + 2a_1C_1 + a_2C_2) \quad (13a)$$

$$\dot{r}_T = \mu - \gamma(r + 2b_1C_1 + 2b_2C_2) \quad (13b)$$

$$0 = \kappa_1 Rr - C_1 \quad (13c)$$

$$0 = \kappa_2 C_1 r - C_2 \quad (13d)$$

$$0 = R + 2C_1 + C_2 - R_T \quad (13e)$$

$$0 = r + 2C_1 + 2C_2 - r_T \quad (13f)$$

Here, $\kappa_1 = \bar{s}_R/K_1$ and $\kappa_2 = \bar{s}_R/K_2$. These parameters are essentially scaled association constants of mRNA-miRNA binding. Based on the estimated range of \bar{s}_R mentioned earlier, and the estimated dissociation constant of mRNA-miRNA binding in the picomolar range (Wee *et al*, 2012), the approximate range of κ_1 and κ_2 is given by $\kappa_1, \kappa_2 = \bar{s}_R/K \in (10^{-9}\text{M}/10^{-11}\text{M}, 10^{-7}\text{M}/10^{-12}\text{M}) = (10^2, 10^5)$.

By eliminating R and r with the conservation relations, the system described in Eq 13 can be simplified with a four-variable system as follows:

$$\dot{R}_T = 1 - (R_T - 2C_1 - C_2) - 2a_1C_1 - a_2C_2 \quad (14a)$$

$$\dot{r}_T = \mu - \gamma(r_T - 2C_1 - 2C_2) - 2\gamma b_1C_1 - 2\gamma b_2C_2 \quad (14b)$$

$$0 = \kappa_1(R_T - 2C_1 - C_2)(r_T - 2C_1 - 2C_2) - C_1 \quad (14c)$$

$$0 = \kappa_2 C_1(r_T - 2C_1 - 2C_2) - C_2 \quad (14d)$$

Eq 14 is useful for performing numerical simulations to capture the system's dynamics, and for stability analysis. However, keeping the variables R_T and r_T makes it difficult to analyze the number of steady states of the system. In addition, the physical constraint $R, r \in \mathbb{R}_{0+}$ must be considered separately in addition to the domains of the four variables. Therefore, we also considered another four-variable system equivalent to Eq 14 describing the steady state of Eq 14 by keeping R and r instead of R_T and r_T :

$$\dot{R}_T = 0 \quad \Leftrightarrow \quad 0 = 1 - (R + 2a_1C_1 + a_2C_2) \quad (15a)$$

$$\dot{r}_T = 0 \quad \Leftrightarrow \quad 0 = \mu - \gamma(r + 2b_1C_1 + 2b_2C_2) \quad (15b)$$

$$0 = \kappa_1 Rr - C_1 \quad (15c)$$

$$0 = \kappa_2 C_1 r - C_2 \quad (15d)$$

Under the tQSSA, replacing the ODEs for R_T and r_T with those for R and r will result in inaccuracy of the dynamics, but Eq 15 accurately describes the steady states of the system. In addition, the condition $R, r, C_1, C_2 \in \mathbb{R}_{0+}$ will directly give $R_T, r_T \in \mathbb{R}_{0+}$, so there is no additional constraint that needs to be considered.

1.8.2 Analysis of the number of steady states

The goal of this section is to find the parameter region in which the system described in Eq 14 has three steady states in \mathbb{R}_{0+} , which are necessary for bistability.

Theorem 1. Suppose $\kappa_1 = \kappa_2 = \kappa \gg a_1/b_2$, $\kappa \gg 1/b_1$, and $a_1, b_1, a_2, b_2 \in \mathbb{R}_{0+}$. There exists a μ ($\mu \in \mathbb{R}_+$) such that Eq 14 has three equilibrium points in \mathbb{R}_{0+}^6 if and only if

$$\frac{a_1}{b_1} < \frac{a_2}{2b_2} \quad (16)$$

Justification of the assumptions: The condition $\kappa_1 = \kappa_2 = \kappa \gg a_1/b_2$ and $\kappa \gg b_1$ means that the formation of the C_1 and C_2 are much more favored than their dissociations. The estimated range of κ is $(10^2, 10^5)$ (1.8.1). It was shown that the fold-changes of degradation rate constants of mRNA and mRNA upon their binding, described with a_1, a_2, b_1 and b_2 , were estimated to be less than one order of magnitude (de la Mata *et al.*, 2015; Eichhorn *et al.*, 2014). We therefore assume that these relationships are justified at least for a significant number of biological systems. In our numerical experiments presented in the next section, we relaxed this assumption and considered a wide range of values for κ (1.8.3).

Proof: We first solve the Eq 15c for C_1 , and we obtain $C_1 = \kappa_1 Rr$. Substituting C_1 with $\kappa_1 Rr$ Eq 15d, and solving the equation for C_2 yields $C_2 = \kappa_1 \kappa_2 Rr^2$. We take the simple assumption $\kappa_1 = \kappa_2 = \kappa$ (no cooperativity in binding), so that $C_2 = \kappa^2 Rr^2$. We then eliminate C_1 and C_2 in Eq 15b, and solve it for R , and we obtain:

$$R = \frac{\eta - r}{2\kappa r(b_1 + 2\kappa b_2 r)}, \quad \text{where } \eta = \frac{\mu}{\gamma} = \frac{s_r k_R^0}{s_R k_r^0} \quad (17)$$

We then eliminate R and C_1 and C_2 in Eq 15a, and we obtain:

$$0 = \kappa^2 a_2 r^3 + (-\kappa^2 a_2 \eta + 2\kappa^2 b_2 + 2\kappa a_1) r^2 + (-2\kappa a_1 \eta + 2\kappa b_1 + 1) r - \eta \quad (18)$$

From $\kappa \gg a_1/b_2$ and $\kappa \gg 1/b_1$, we obtain $2\kappa^2 b_2 + 2\kappa a_1 \cong 2\kappa^2 b_2$, and $2\kappa b_1 + 1 \cong 2\kappa b_1$. Eq 18 can therefore be approximated by:

$$0 = \kappa^2 a_2 r^3 + (-\kappa^2 a_2 \eta + 2\kappa^2 b_2) r^2 + (-2\kappa a_1 \eta + 2\kappa b_1) r - \eta \quad (19)$$

We next use an algebraic geometry approach to find the conditions under which Eq 19 has three real positive equilibrium points (Siegal-Gaskins *et al*, 2015).

We first define the right-hand side of Eq 19 as $P(x)$, i.e.:

$$P(r) = \kappa^2 a_2 r^3 + (-\kappa^2 a_2 \eta + 2\kappa^2 b_2) r^2 + (-2\kappa a_1 \eta + 2\kappa b_1) r - \eta \quad (20)$$

We then construct the Sturm sequence for $P(x)$, i.e. a set of polynomials defined as:

$$\begin{aligned} P_0 &= P, \\ P_1 &= P_0', \\ P_2 &= -\text{rem}(P_1, P_0), \\ P_3 &= -\text{rem}(P_2, P_1) \end{aligned} \quad (21)$$

Here, $\text{rem}(P_{i-1}, P_i)$ is the remainder of the polynomial long division of P_i by P_{i-1} . It follows Sturm's theorem that $P(r)$ has three real roots in interval $(0, \infty)$ if and only if $V(0) - V(\infty) = 3$ where V is number of sign variations in the sequence Eq 21. The sequence has four elements, therefore $V(0) \leq 3$, and since $V(\infty) \geq 0$, $P(r)$ has three real positive roots if and only if the sequence Eq 21 satisfies $V(0) = 3$ and $V(\infty) = 0$.

We calculate the Sturm sequence as follows:

$$\begin{aligned} P_0 &= \kappa^2 a_2 r^3 - (a_2 \eta - 2b_2) \kappa^2 r^2 - 2(a_1 \eta - b_1) \kappa r - \eta \\ P_1 &= 3\kappa^2 a_2 r^2 - 2(a_2 \eta - 2b_2) \kappa^2 r - 2\kappa(a_1 \eta - b_1) \\ P_2 &= 2(2\kappa(a_2 \eta - 2b_2)^2 + 6a_2(a_1 \eta - b_1)) \kappa^5 r + 2a_2(a_1 \eta - b_1)(a_2 \eta - 2b_2) \kappa^5 + 9\kappa^4 a_2^2 \eta \\ P_3 &= 36a_2^3(a_2 \eta - 2b_2)^2((a_1 \eta - b_1)^2 - \eta(a_2 \eta - 2b_2)) \kappa^{12} + O(\kappa^{11}) \end{aligned} \quad (22)$$

Since $\lim_{r \rightarrow \infty} P_0(r) = \infty$ and $P_0(0) = -\eta < 0$, the only combination of signs in the sequences that allow three real positive roots is the following:

	P_0	P_1	P_2	P_3
$r = 0$	-	+	-	+
$r \rightarrow \infty$	+	+	+	+

We next look for the conditions in terms of the parameters that satisfy all signs shown above by enumerating the remaining six inequalities with respect to P_1 , P_2 and P_3 .

From Eq 22 we first obtain $\lim_{r \rightarrow \infty} P_1(r) = \infty > 0$. In addition, $P_1(0) > 0$ if and only if

$$a_1 \eta - b_1 < 0 \quad (23)$$

From the assumption $\kappa \gg 1/b_1$, we obtain

$$\begin{aligned}
P_2(0) &= 2a_2(a_1\eta - b_1)(a_2\eta - 2b_2)\kappa^5 + 9\kappa^4 a_2^2 \eta \\
&= 2a_2(a_1\eta - b_1)(a_2\eta - 2b_2)\kappa^5
\end{aligned} \tag{24}$$

Similarly, $\lim_{r \rightarrow \infty} P_2(r) = \infty > 0$. With Eq 23, $P_2(0) < 0$ if and only if

$$a_2\eta - 2b_2 > 0 \tag{25}$$

From Eq 23 and Eq 25, we conclude that there exists a μ ($\mu \in \mathbb{R}_+$) such that $a_1\eta - b_1 < 0$ and $a_2\eta - 2b_2 > 0$ if and only if Eq 16 is satisfied.

From Eq 22, we get:

$$\text{sgn}(P_3(r)) = \text{sgn}((a_1\eta - b_1)^2 - \eta(a_2\eta - 2b_2)) \tag{26}$$

Because when $2b_2/a_2 = \eta$,

$$(a_1\eta - b_1)^2 - \eta(a_2\eta - 2b_2) = (a_1\eta - b_1)^2 > 0 \tag{27}$$

There exists an $\eta^* \in (2b_2/a_2, b_1/a_1)$, such that for all $\eta \in (2b_2/a_2, \eta^*)$, $\text{sgn}(P_3(r)) > 0$ if and only if Eq 16 is satisfied. Eq 16 is therefore the necessary and sufficient condition for Eq 15, and equivalently Eq 14, to have three real positive equilibrium points if $\kappa_1 = \kappa_2 = \kappa \gg a_1/b_2$, $\kappa \gg 1/b_1$, and $a_1, b_1, a_2, b_2 \in \mathbb{R}_{0+}$.

We next eliminate the possibility that one of the four variables in Eq 15 can be zero in the solutions. Because $\mu \in \mathbb{R}_+$, $r = 0$ is not a solution to Eq 19. From Eq 15c and Eq 15d, we obtain:

$$R = 0 \Leftrightarrow C_1 = 0 \Leftrightarrow C_2 = 0 \tag{28}$$

This does not satisfy Eq 15a. Therefore, when Eq 14 is at steady state, $r, R, C_1, C_2 \neq 0$. \square

We next show that if Eq 16 is satisfied, the system described in Eq 14 switches from one equilibrium point, to three equilibrium point, then to one equilibrium point again when η increases from zero to a number greater than b_1/a_1 .

If $0 < \eta < 2b_2/a_2 < b_1/a_1$, the signs of Sturm sequences of $P(r)$ are $\{-, +, +, +\}$ and $\{+, +, +, +\}$ for $r = 0$ and $r \rightarrow \infty$, respectively. Therefore $V(0) - V(\infty) = 1$, i.e. Eq 15 has only one solution. In addition, if $\eta > b_1/a_1 > 2b_2/a_2$, the signs of Sturm sequences of $P(r)$ are $\{-, -, +, U\}$ and $\{+, +, +, U\}$ for $r = 0$ and $r \rightarrow \infty$, respectively, where U is an undetermined sign. Therefore $V(0) - V(\infty) = 1$, i.e. Eq 15 has only one solution.

1.8.3 Numerical experiments for bistable switches

Theorem 1 and the conclusion stated above may offer a simple framework for obtaining bistable switches with Eq 14, but they do not provide information about stability of the system Eq 14. Typical bistable switches require that in the parameter region with three steady states, two of the steady states are stable (stable nodes) and the remaining one is unstable (saddle point). In this scenario, changes in parameters allows the system to switch between three-steady-state region and one-steady state region via saddle-node bifurcations. However, we cannot make these conclusions based on the analysis described in 1.8.2. Although linear stability analysis under a limiting condition ($\kappa \rightarrow \infty$) provided some insights into stability (not shown), we were not able to obtain conclusive results about the stability for each of the three steady

states. This implies that bifurcations other than saddle-node are possible with Eq 14. Here, we present numerical experiments that serve at least four purposes: 1) they validate conclusions of Theorem 1; 2) they show stability of each steady state in systems with various parameter sets; 3) they show the biochemical interpretations of off-state and on-state of the system and 4) they show the performance of Eq 16 in predicting the bistability of the system Eq 14 when the assumption about association constant κ is relaxed.

With the system described in Eq 14, we first chose a large association constant κ ($\kappa = 10^5$, i.e. the upper bound of our estimate in biological systems) that would satisfy the assumption of Theorem 1. We assumed that the basal degradation rate constant of miRNA is equal to that of the mRNA ($\gamma = 1$). For the relative degradation rate constants a_1, b_1, a_2, b_2 , we selected 10^4 sets of values from uniformly distributed random numbers over the interval $(1/8, 16)$. These bounds were estimated from the altered stability of mRNA induced by miRNA binding, as well as the altered stability of miRNA induced by mRNA binding (de la Mata *et al.*, 2015; Eichhorn *et al.*, 2014). For each of the 10^4 parameter sets, we performed one-parameter numerical bifurcation analysis with $\eta = 0$ as the starting point of control parameter. Unsurprisingly, letting $\eta = 0$ gave rise to a stable steady state where $r_T = 0$ and $R_T > 0$ with each parameter set. We define a system as a bistable switch if it has two saddle-node bifurcation points at two distinct values of η , which bound a region containing two stable nodes and one saddle point.

To compare the analytical prediction of bistability with Eq 16 with the results from the numerical experiments, we treated Eq 16 as a ‘predictor’ of bistable systems, and the numerically revealed bistable systems as ‘true’ bistable systems. This notion may be counterintuitive because analytical solutions are often used to evaluate numerical methods. In our case, the analytical conclusion serves as a guide to conduct numerical experiments and to derive intuitions of the feedback in this system, but the analysis involves a key biological assumption that needs to be evaluated and relaxed in biological applications. The detection capacity of the numerical method is limited by its precision, but the inaccuracy is neglected here. Among the 10^4 parameter sets (referred to as models), 3391 of them were predicted to bistable according to inequality Eq 16, and the remaining models were predicted to be monostable. 98.73% or 3348 of these predicted bistable systems were confirmed numerically, resulting in 43 false positives (numerically determined as monostable systems). Among the 6609 models that were predicted monostable according to the inequality Eq 16, 97.55% or 6527 of them were determined to be monostable numerically. The confusion matrix is shown in Table S2. Interestingly, 0.12% of the 10^4 parameter sets generated Hopf bifurcation point in addition to saddle-node bifurcation points, so that two of the three coexisting steady states are unstable. Since these systems are rare, we did not exclude them from the true bistable population, nor did we perform further analysis of these rare cases in this study.

Table S2. Confusion matrix for analytical prediction of bistable systems and numerical validations

	Predicted monostable	Predicted bistable
Monostable with numerical bifurcation	6527 (TP)	43 (FP)
bistable with numerical bifurcation	9 (FN)	3348 (TN)

TP: True positive. FP: False positive. FN: False negative. TN: True negative.

With visual inspection of the bifurcation diagrams of the numerically validated bistable systems (Figure 5C), we found that variables r_T, R_T, r, R and C_2 exhibited clear switches between on and off states with changes of η in most cases. This suggests that these bistable switches may be biochemical functional. Unsurprisingly, for r_T and R_T , the difference between on and off state is within one order of magnitude in

most cases. In contrast, the on-off difference for r, R is typically greater than two orders of magnitude (Figure 5C). We found that similar fractions of parameter sets gave rise to bistable systems when we selected parameter values for a_1, b_1, a_2, b_2 from an interval other than $(1/8, 16)$, e.g. $(1, 16)$ or $(1/8, 1)$, and when we selected a_1, a_2 and b_1, b_2 from distinct intervals (Figure S4). Under these constraints of parameters, switch-like behaviors were also obtained with molecules such as r, R (Figure S5).

Under the basal parameter setting ($\kappa = 10^5$), we obtained 99.48% accuracy, 99.74% true positive rate, and 99.76% true negative rate using Eq 16 as a predictor for bistability. We next asked how this performance would change with the decrease of κ , i.e. relaxing the assumption of Theorem 1. We therefore repeated this numerical experiment with various values of κ (Figure S6A, pink, green, gold and purple). Furthermore, we found that the true positive rate was robust to the decrease of κ , whereas the true negative rate decreased as κ decreased (Figure S6A, green, and purple). Nonetheless, with a moderately high association constant ($\kappa = 10^2$) that is the lower bound of our estimate in biological systems (1.8.1), the accuracy and true negative rate were still higher than 90% (Figure S6A, gold, and purple), indicating that Eq 16 serves as a reasonable predictor of biological bistable systems governed by kinetics described in Eq 14. Furthermore, nearly 30% of the randomly selected parameter sets gave rise to bistable systems under this assumption of κ (Figure S6A, pink). Even with a low association constant ($\kappa = 1$), about three percent of the randomly generated parameter sets generated bistable systems (Figure S6A, pink), which were correctly predicted by Eq 16. These results suggest that the reaction network described in Eq 14 may be a widely used motif for generating bistable switches in biology. In addition, we found that restricting a_1, b_1, a_2, b_2 to $(1/8, 1)$ or $(1, 16)$ reduced the fractions of parameter sets that generated bistable systems, but the decrease was not dramatic (Figure S6, cyan and yellow).

1.9 mRNA-miRNA model with three binding sites (mmi-3 Model)

The mRNA-miRNA model with three binding sites is simply an extension of the mmi-2 Model. We expanded Eq 14, a simplified system for the mmi-2 Model, by adding an equation for C_3 , a partially double-stranded complex formed by three miRNA molecules bound to an mRNA molecule:

$$\dot{R}_T = 1 - (R_T - 3C_1 - 3C_2 - C_3) - 3a_1C_1 - 3a_2C_2 - a_3C_3 \quad (29a)$$

$$\dot{r}_T = \eta - (r_T - 3C_1 - 6C_2 - 3C_3) - 3b_1C_1 - 6b_2C_2 - 3b_3C_3 \quad (29b)$$

$$0 = \kappa_1(R_T - 3C_1 - 3C_2 - C_3)(r_T - 3C_1 - 6C_2 - 3C_3) - C_1 \quad (29c)$$

$$0 = \kappa_2C_1(r_T - 3C_1 - 6C_2 - 3C_3) - C_2 \quad (29d)$$

$$0 = \kappa_3C_2(r_T - 3C_1 - 6C_2 - 3C_3) - C_3 \quad (29e)$$

We performed numerical experiments similar to those described in 1.8.3. Values for relative degradation rate constants $a_1, b_1, a_2, b_2, a_3, b_3$ were randomly selected from the interval $(1/8, 16)$. With numerical bifurcation analysis with respect to η using 10^4 parameter sets, we found that a high association constant ($\kappa = 10^5$) gave rise to 5081 bistable systems, whereas a moderately high association constant ($\kappa = 10^2$) gave rise to 4022 bistable systems (Figure S6A, blue and S6B). The distributions of individual parameters from bistable systems were wider than those from mmi-2 bistable systems (Figure S6B). These results show that with the increased number of binding sites, it is even more feasible for the system to achieve bistability with biologically plausible kinetic rate constants.

549 1.10 Estimate of realistic biological circuits described by mmi-2 and mmi-3 Models

550 To estimate how frequently the mRNA-miRNA reaction network motif represented by mmi-2 and mmi-3
551 models can be found in biological systems, we obtained a data set for predicted miRNA binding sites in
552 human and mouse from TargetScan (Agarwal *et al*, 2015). To estimate the lower bound of the number of
553 appearances, we counted the number of mRNA-miRNA pairs in which the target mRNA has two or more
554 conserved binding sites for the cognate miRNA. To estimate the upper bound, we counted the number of
555 miRNA binding site duplets or triplets (conserved and non-conserved) each of which share target mRNA
556 and cognate miRNA. The numbers of predicted target gene, cognate miRNA and mRNA-miRNA circuit
557 are listed in Table 1.

558
559 1.11 mRNA-miRNA with noncanonical feedback and morphogen gradients (mmi-S
560 Model)
561

562 The form of equation is identical to Tmi-UR model (Eq2, Eq 4 and Eq 5). The parameters were chosen
563 based on the principle derived in 1.8 and 1.9 (mmi-2 and mmi-3 models), such that both Hoxa5-miR-27
564 axis and Hoxc8-miR-196 axis are bistable. The parameter values of this and other models are listed in Table
565 S3 and Table S4.

566
567 1.12 List of parameter values and ranges for random sampling
568
569

Table S3. List of parameter values and ranges for random sampling

Parameter	Description	Value in T-CR	Value in T-UR	Value in Tmi-UR	Value in Tmi-FB	Sampling Range *	Value in mmi-S
s_5^0	Basal production rate constant of <i>Hoxa5</i> mRNA	0	0	0.15	0.15	$\mu=0.01, \sigma=1.5$	0.06
s_5	Regulated production rate constant of <i>Hoxa5</i> mRNA	1	1	1	1	$\mu=10, \sigma=1.5$	2
K_{5A}	Threshold of <i>Hoxa5</i> activation by RA	0.7	0.7	0.98	0.48	$\mu=1, \sigma=0.5$	7.2
n_{5A}	Response nonlinearity of <i>Hoxa5</i> activation by RA	6	60 **	6	6	6	2
K_{58}	Threshold of <i>Hoxa5</i> inhibition by Hoxc8	0.05	0.05	0.1	0.05	$\mu=0.1, \sigma=1.5$	0.006
n_{58}	Response nonlinearity of <i>Hoxa5</i> inhibition by Hoxc8	6	20 **	40 **	6	6	2
s_8^0	Basal production rate constant of <i>Hoxc8</i> mRNA	0	0	0.05	0	$\mu=0.01, \sigma=1.5$	0
s_8	Regulated production rate constant of <i>Hoxc8</i> mRNA	1	1	1	1	$\mu=10, \sigma=1.5$	1.2
K_{8F}	Threshold of <i>Hoxc8</i> activation by FGF	0.3	0.75	0.95	2.3	$\mu=1, \sigma=0.5$	0.95
n_{8F}	Response nonlinearity of <i>Hoxc8</i> activation by FGF	6	60 **	40 **	6	6	6
K_{85}	Threshold of <i>Hoxc8</i> inhibition by Hoxa5	NA	0.18	NA	NA	$\mu=0.1, \sigma=1.5$	NA
n_{85}	Response nonlinearity of <i>Hoxc8</i> inhibition by Hoxa5	NA	6	NA	NA	6	NA
l_5^0	Translation rate constant of free <i>Hoxa5</i> mRNA	1	1	1	1	$\mu=2, \sigma=1$	1.8
l_8^0	Translation rate constant of free <i>Hoxc8</i> mRNA	0.7	1	1	5	$\mu=2, \sigma=1$	3.9
k_5	Degradation rate constant of free <i>Hoxa5</i> mRNA	1	1	1	1	1	1
k_8	Degradation rate constant of free <i>Hoxc8</i> mRNA	1	1	1	1	1	1
k_5^i	Degradation rate constant of <i>Hoxa5</i> mRNA in complex C_5^i	NA	NA	1	3	$\mu=2, \sigma=1.5$	Table S4
k_8^i	Degradation rate constant of <i>Hoxc8</i> mRNA in complex C_8^i	NA	NA	1	1	$\mu=2, \sigma=1.5$	Table S4
l_5^i	Translation rate constant of complex C_5^i	NA	NA	0	0	0	0
l_8^i	Translation rate constant of complex C_8^i	NA	NA	0	0	0	0
K_{2A}	Threshold of miR-27 inhibition by RA	NA	NA	0.9	0.9	$\mu=1, \sigma=0.5$	3.2
n_{2A}	Response nonlinearity of miR-27 inhibition by RA	NA	NA	6	6	6	6
k_2	Regulated production rate constant of miR-27	NA	NA	1	1	$\mu=1, \sigma=1.5$	0.16
k_9	Regulated production rate constant of miR-196	NA	NA	1	1	$\mu=1, \sigma=1.5$	0.8
k_2^i	Degradation rate constant of miR-27 in complex C_5^i	NA	NA	1	1	$\mu=1, \sigma=1.5$	Table S4
k_9^i	Degradation rate constant of miR-196 in complex C_8^i	NA	NA	1	1	$\mu=1, \sigma=1.5$	Table S4
κ_5^i	Association constant of complex C_5^i formation	1000	1000	1000	1000	1000	1000
κ_8^i	Association constant of complex C_8^i formation	1000	1000	1000	1000	1000	1000
K_{25}	Threshold of miR-27 inhibition by Hoxa5	NA	NA	NA	0.1	$\mu=0.1, \sigma=1.5$	NA
n_{25}	Response nonlinearity of miR-27 inhibition by Hoxa5	NA	NA	NA	6	6	NA
K_{98}	Threshold of miR-196 inhibition by Hoxc8	NA	NA	NA	0.02	$\mu=0.1, \sigma=1.5$	NA
n_{98}	Response nonlinearity of miR-196 inhibition by Hoxc8	NA	NA	NA	6	6	NA

571

572

573

574

* Parameter values were assumed to be constants, or randomly drawn from log-normal distributions with the indicated μ and σ . All models use the same distributions, where the parameters are applicable.

** Extremely high nonlinearity was assumed to estimate the upper bound of the performance.

575

Table S4. Additional parameter values for mmi-S Model

Parameter	Description	Value in mmi-S Model
k_5^1	Degradation rate constant of <i>Hoxa5</i> mRNA in complex C_5^1	0.3
k_5^2	Degradation rate constant of <i>Hoxa5</i> mRNA in complex C_5^2	0.53
k_5^3	Degradation rate constant of <i>Hoxa5</i> mRNA in complex C_5^3	1.53
k_8^1	Degradation rate constant of <i>Hoxc8</i> mRNA in complex C_8^1	1
k_8^2	Degradation rate constant of <i>Hoxc8</i> mRNA in complex C_8^2	1
k_8^3	Degradation rate constant of <i>Hoxc8</i> mRNA in complex C_8^3	1.5
k_8^4	Degradation rate constant of <i>Hoxc8</i> mRNA in complex C_8^4	2.66
k_2^1	Degradation rate constant of miR-27 in complex C_5^1	1
k_2^2	Degradation rate constant of miR-27 in complex C_5^2	1
k_2^3	Degradation rate constant of miR-27 in complex C_5^3	0.6
k_9^1	Degradation rate constant of miR-196 in complex C_8^1	2.7
k_9^2	Degradation rate constant of miR-196 in complex C_8^2	2.1
k_9^3	Degradation rate constant of miR-196 in complex C_8^3	0.75
k_9^4	Degradation rate constant of miR-196 in complex C_8^4	0.12

576 * The bifurcation diagram shown in Figure 7H were produced under the same parameter settings as the mmi-S Model, except for the following
577 parameters: $l_5^0 = 0.03$, $l_5^1 = 0.5$, $K_{5A} = 0.7$, $n_{5A} = 6$, $K_{2A} = 0.6$. The mmi-S Model under with these parameter values produced results similar to
578 those shown in Figure 8.

579

580 As described in 1.6, model parameters were first randomly chosen from defined distributions which are
581 consistent across all models. Model evaluations are based on statistics obtained from the parameter
582 sampling. To show representative simulation results, we chose one parameter set for each model and
583 adjusted some parameters manually for illustration purposes. The range of parameter sampling and the
584 parameter values of representative models are listed in Table S3 and Table S4.

585

586 **2. Additional Information of Resources**

587 **2.1 List of key reagents and resources**

588 **Table S5. List of key reagents and resources**

Reagent type (species) or resource	Designation	Source or reference	Identifiers	Additional information
Antibody	Goat anti-Isl1	Neuromics	Cat# 39.4D5, RRID: AB_2314682	ICC (1:1000)
Antibody	Mouse monoclonal anti-Isl1(2)	DSHB	Cat# 39.4D5, RRID: AB_2314683	ICC (1:1000)
Antibody	Rabbit polyclonal anti-Hoxa5	Jeremy Dasen (NYU)		ICC (1:16000)
Antibody	Guinea pig polyclonal pig anti-Hoxa5	Jun-An Chen (Academia Sinica)	RRID: AB_2744661	ICC (1:20000)

Antibody	Mouse monoclonal anti-Hoxc8	DSHB	Cat# PCRP-HOXC8-1D3, RRID: AB_2618723	ICC (1:1000)
Antibody	Rabbit polyclonal anti-Hoxc8	Sigma-Aldrich	Cat# HPA028911, RRID: AB_10602236	ICC (1:5000)
Antibody	Sheep polyclonal anti-GFP	AbD Serotec	Cat# 4745-1051, RRID: AB_619712	ICC (1:1000)
Antibody	Guinea pig polyclonal anti-Hb9	Hynek Wichterle (Columbia University)		ICC (1:1000)
Antibody	Mouse monoclonal anti-Hb9	DSHB	Cat# 81.5C10, RRID: AB_2145209	ICC (1:200)
Cell line	Mouse: <i>Hb9::GFP</i> (<i>Mnx1::GFP</i>) ESCs	(Wichterle <i>et al.</i> , 2002)		Dr. Hynek Wichterle (Columbia University)
Mouse strain	<i>Hoxc8::Cre</i>	(Carroll & Capecchi, 2015)		Dr. Mario Capecchi (University of Utah)
Mouse strain	<i>ROSA26-loxp-STOP-loxp-tdTomato</i>	(Madisen <i>et al.</i> , 2010)	The Jackson Lab (Stock No. 007914)	Dr. Hong-Kui Zeng (Allen Institute)
Cell line	Mouse: <i>iHoxa5-V5</i> ESCs	this study		
Cell line	Mouse: <i>iHoxc8-V5</i> ESCs	(Li <i>et al.</i> , 2017)		
Cell line	Mouse: <i>imiR-ScrmSP</i> ESCs	(Li <i>et al.</i> , 2017)		
Cell line	Mouse: <i>imiR-27SP</i> ESCs	(Li <i>et al.</i> , 2017)		
Cell line	Mouse: <i>iGFP</i> ESCs	(Li <i>et al.</i> , 2017)		
Cell line	Mouse: <i>imiR-196a OE</i> ESCs	this study		
Cell line	Mouse: <i>imiR-27b OE</i> ESCs	this study		
Mouse strain	<i>Hb9::GFP</i>	(Wichterle <i>et al.</i> , 2002)		
Mouse strain	<i>miR-23a~27a~24-2^{+/-}; miR-23b~27b~24-1^{+/-}</i>	(Li <i>et al.</i> , 2017)		
Mouse strain	<i>miR-196a1^{+/-}; miR-196a2^{-/-}; miR-196b^{-/-}</i>	(Wong <i>et al.</i> , 2015)		
<i>In situ</i> probe	mmu-Hoxa5	(Li <i>et al.</i> , 2017)		

<i>In situ</i> probe	mmu-Hoxc8	(Li <i>et al.</i> , 2017)		
<i>In situ</i> probe	mmu-miR-27b	QIAGEN	MIMAT0000126	
Commercial assay or kit	Neural Tissue Dissociation Kit (P)	Miltenyi Biotec	130-092-628	
Commercial assay or kit	Chromium Single Cell 3' Reagent Kits v3.1	10X Genomics	PN-1000121	
Software, algorithm	10X Cell Ranger v3.1.0	10X Genomics	RRID: SCR_017344	
Software, algorithm	Seurat v2.3.4	(Butler <i>et al.</i> , 2018; Stuart <i>et al.</i> , 2019)	RRID: SCR_016341	
Software, algorithm	MetaMorph Microscopy Automation and Image Analysis Software		RRID: SCR_002368	
Software, algorithm	Differential Equation Solver: Differentialequations.jl 6.14.0	(Rackauckas & Nie, 2017)		
Software, algorithm	Numerical Bifurcation Analysis: Tellurium 2.1.5, AUTO	(Choi <i>et al.</i> , 2018; Doedel, 1981)		

589

590 2.2 Primers for genotyping

591

Table S6. Primers for genotyping

Gene	Forward Primer	Reverse Primer
GFP	CCCTGAAGTTCATCTGCACCAC	TTCTCGTTGGGGTCTTTGCTC
Cre	TGATGGACATGTTCAGGGATC	CAGCCACCAGCTTGCATGA
Ai14 WT	AAGGGAGCTGCAGTGGAGTA	CCGAAAATCTGTGGGAAGTC
Ai14 Mutant	CTGTTCTGTACGGCATGG	GGCATTAAGCAGCGTATCC
miR-27a WT	GGGAATGCTTCTTCCCTCTT	CACGACTTTGCTGTGGACCT
miR-27a Del	GGGAATGCTTCTTCCCTCTT	CTATCTGCTTTGGGGAACCA
miR-27b WT	CTCTGTGCTATGCCTCAGCTTAT	CCCCATCTCACCTTCTCTTCAG
miR-27b Del	CTCTGTGCTATGCCTCAGCTTAT	TCAGAAAGGCTCTACAGACAAGG

592

593 2.3 Sequence for miRNA sponge

594

595 miR-27b sponge (8 repeats, ccgg as spacer)

596 5'

597 GCAGAACTTCGGACTGTGAAccggGCAGAACTTCGGACTGTGAAccggGCAGAACTTCGGACTG
598 TGAAccggGCAGAACTTCGGACTGTGAAccggGCAGAACTTCGGACTGTGAAccggGCAGAACTT
599 CGGACTGTGAAccggGCAGAACTTCGGACTGTGAAccggGCAGAACTTCGGACTGTGAA

600 mir-scramble sponge (8 repeats, ccgg as spacer)

601 5'

602 TTCACAATGCGTTATCGGATGTccggTTCACAATGCGTTATCGGATGTccggTTCACAATGCGTT
603 ATCGGATGTccggTTCACAATGCGTTATCGGATGTccggTTCACAATGCGTTATCGGATGTccggT
604 TCACAATGCGTTATCGGATGTccggTTCACAATGCGTTATCGGATGTccggTTCACAATGCGTTA
605 TCGGATGT

606

Supplemental References

- Agarwal V, Bell GW, Nam J-W, Bartel DP (2015) Predicting effective microRNA target sites in mammalian mRNAs. *elife* 4: e05005
- Borghans JAM, De Boer RJ, Segel LA (1996) Extending the quasi-steady state approximation by changing variables. *Bull Math Biol* 58: 43-63
- Butler A, Hoffman P, Smibert P, Papalexi E, Satija R (2018) Integrating single-cell transcriptomic data across different conditions, technologies, and species. *Nat Biotechnol* 36: 411-420
- Carroll LS, Capecchi MR (2015) Hoxc8 initiates an ectopic mammary program by regulating Fgf10 and Tbx3 expression and Wnt/beta-catenin signaling. *Development* 142: 4056-4067
- Choi K, Medley JK, König M, Stocking K, Smith L, Gu S, Sauro HM (2018) Tellurium: an extensible python-based modeling environment for systems and synthetic biology. *Biosystems* 171: 74-79
- Ciliberto A, Capuani F, Tyson JJ (2007) Modeling networks of coupled enzymatic reactions using the total quasi-steady state approximation. *PLoS Comput Biol* 3: e45
- Dasen JS, Tice BC, Brenner-Morton S, Jessell TM (2005) A Hox regulatory network establishes motor neuron pool identity and target-muscle connectivity. *Cell* 123: 477-491
- de la Mata M, Gaidatzis D, Vitanescu M, Stadler MB, Wentzel C, Scheiffele P, Filipowicz W, Großhans H (2015) Potent degradation of neuronal miRNAs induced by highly complementary targets. *EMBO Rep* 16: 500-511
- Doedel EJ (1981) AUTO: A program for the automatic bifurcation analysis of autonomous systems. *Congr Numer* 30: 265-284
- Eichhorn SW, Guo H, McGeary SE, Rodriguez-Mias RA, Shin C, Baek D, Hsu S-h, Ghoshal K, Villén J, Bartel DP (2014) mRNA destabilization is the dominant effect of mammalian microRNAs by the time substantial repression ensues. *Mol Cell* 56: 104-115
- Ensini M, Tsuchida TN, Belting H-G, Jessell TM (1998) The control of rostrocaudal pattern in the developing spinal cord: specification of motor neuron subtype identity is initiated by signals from paraxial mesoderm. *Development* 125: 969-982
- Feinberg M (2019) *Foundations of Chemical Reaction Network Theory*. Springer International Publishing
- Ghini F, Rubolino C, Climent M, Simeone I, Marzi MJ, Nicassio F (2018) Endogenous transcripts control miRNA levels and activity in mammalian cells by target-directed miRNA degradation. *Nat Commun* 9: 3119
- Grimson A, Farh KK-H, Johnston WK, Garrett-Engele P, Lim LP, Bartel DP (2007) MicroRNA targeting specificity in mammals: determinants beyond seed pairing. *Mol Cell* 27: 91-105
- Kloosterman WP, Wienholds E, de Bruijn E, Kauppinen S, Plasterk RHA (2006) In situ detection of miRNAs in animal embryos using LNA-modified oligonucleotide probes. *Nat Methods* 3: 27-29

642 Lahtvee P-J, Sánchez BJ, Smialowska A, Kasvandik S, Elseman IE, Gatto F, Nielsen J (2017) Absolute
643 quantification of protein and mRNA abundances demonstrate variability in gene-specific translation
644 efficiency in yeast. *Cell systems* 4: 495-504

645 Li C-J, Hong T, Tung Y-T, Yen Y-P, Hsu H-C, Lu Y-L, Chang M, Nie Q, Chen J-A (2017) MicroRNA
646 filters Hox temporal transcription noise to confer boundary formation in the spinal cord. *Nat Commun* 8:
647 14685

648 Lu M, Jolly MK, Levine H, Onuchic JN, Ben-Jacob E (2013) MicroRNA-based regulation of epithelial-
649 hybrid-mesenchymal fate determination. *Proc Natl Acad Sci U S A*

650 Madisen L, Zwingman TA, Sunkin SM, Oh SW, Zariwala HA, Gu H, Ng LL, Palmiter RD, Hawrylycz
651 MJ, Jones AR *et al* (2010) A robust and high-throughput Cre reporting and characterization system for
652 the whole mouse brain. *Nat Neurosci* 13: 133-140

653 Mazzoni EO, Mahony S, Peljto M, Patel T, Thornton SR, McCuine S, Reeder C, Boyer LA, Young RA,
654 Gifford DK (2013) Saltatory remodeling of Hox chromatin in response to rostrocaudal patterning signals.
655 *Nat Neurosci* 16: 1191-1198

656 Osella M, Bosia C, Corá D, Caselle M (2011) The role of incoherent microRNA-mediated feedforward
657 loops in noise buffering. *PLoS Comput Biol* 7: e1001101

658 Philippidou P, Dasen JS (2013) Hox genes: choreographers in neural development, architects of circuit
659 organization. *Neuron* 80: 12-34

660 Rackauckas C, Nie Q (2017) Differentialequations. jl—a performant and feature-rich ecosystem for
661 solving differential equations in julia. *Journal of Open Research Software* 5

662 Siegal-Gaskins D, Franco E, Zhou T, Murray RM (2015) An analytical approach to bistable biological
663 circuit discrimination using real algebraic geometry. *Journal of The Royal Society Interface* 12: 20150288

664 Sosnik J, Zheng L, Rackauckas CV, Digman M, Gratton E, Nie Q, Schilling TF (2016) Noise modulation
665 in retinoic acid signaling sharpens segmental boundaries of gene expression in the embryonic zebrafish
666 hindbrain. *Elife* 5: e14034

667 Stuart T, Butler A, Hoffman P, Hafemeister C, Papalexi E, Mauck Iii WM, Hao Y, Stoeckius M, Smibert
668 P, Satija R (2019) Comprehensive integration of single-cell data. *Cell* 177: 1888-1902

669 Tian XJ, Zhang H, Zhang J, Xing J (2016) Reciprocal regulation between mRNA and microRNA enables
670 a bistable switch that directs cell fate decisions. *FEBS Lett* 590: 3443-3455

671 Wee LM, Flores-Jasso CF, Salomon WE, Zamore PD (2012) Argonaute divides its RNA guide into
672 domains with distinct functions and RNA-binding properties. *Cell* 151: 1055-1067

673 Wichterle H, Lieberam I, Porter JA, Jessell TM (2002) Directed differentiation of embryonic stem cells
674 into motor neurons. *Cell* 110: 385-397

675 Wong SFL, Agarwal V, Mansfield JH, Denans N, Schwartz MG, Prosser HM, Pourquie O, Bartel DP,
676 Tabin CJ, McGlinn E (2015) Independent regulation of vertebral number and vertebral identity by
677 microRNA-196 paralogs. *Proc Natl Acad Sci USA* 112: E4884-E4893